(Received 1 April 2025, Accepted 12 June 2025, Scheduled 15 July 2025)

Designing MIMO Antenna with High Isolation Decoupling Structure

Jyoti C. Kolte*, Ashwini Kumar, and Payal Bansal

Poornima University, Jaipur, India

ABSTRACT: This paper presents the design and development of a miniaturized Multiple-Input Multiple-Output (MIMO) antenna for sub-6 GHz 5G applications, featuring reduced cross polarization and enhanced isolation between antenna elements. Utilizing characteristics mode analysis, slots are introduced in the patch to achieve orthogonal mode separation, effectively minimizing cross polarization. Further bandwidth enhancement is achieved by incorporating slot loading in the ground plane. To improve isolation between antenna elements, spiral decoupling (SD) and aperture spiral decoupling (ASD) structures are employed. The proposed MIMO antenna, with dimensions $0.32\lambda_o * 0.32\lambda_o * 0.01\lambda_o$ where λ_o is the wavelength at the lower band frequency of 3.5 GHz, was fabricated and experimentally tested to validate its performance. Measurement results indicate significant compactness, low envelope correlation coefficient (ECC), high gain, minimal channel capacity loss, and very low mutual coupling between elements. The measured results are in good agreement with simulated ones, confirming that the proposed antenna is a promising candidate for advanced MIMO applications in next-generation wireless communication systems.

1. INTRODUCTION

The evolution of wireless communication systems has accelerated rapidly, driven by the need for higher data rates, greater capacity, and improved reliability. As the world transitions to the fifth generation (5G) of wireless technology, these requirements become even more critical. 5G technology promises enhanced mobile broadband, ultra-reliable low-latency communication, and massive machine-type communication, making it a cornerstone for future smart applications, including the Internet of Things (IoT), autonomous vehicles, and advanced healthcare systems [1–5].

Among the various frequency bands allocated for 5G, the sub-6 GHz band is particularly significant due to its balance between coverage and capacity. This band offers better propagation characteristics and penetration capabilities than millimeter-wave bands, making it suitable for widespread urban and rural deployments. However, designing antennas for sub-6 GHz 5G applications presents unique challenges, particularly in achieving compact size, wide bandwidth, and high isolation between multiple antenna elements in a MIMO configuration [6–10].

MIMO technology is a critical enabler for 5G, leveraging multiple antennas at both the transmitter and receiver ends to improve communication performance. MIMO systems enhance spectral efficiency, data rates, and link reliability through spatial diversity and multiplexing gains. For effective MIMO operation, antennas must exhibit low mutual coupling, high isolation, and minimal cross polarization to ensure independent and efficient operation of each element. One of the primary challenges in MIMO antenna design is miniaturization. As devices become smaller, the demand for compact antennas that can fit within limited spaces increases. Traditional antenna designs often face difficulties in maintaining performance metrics such as impedance bandwidth, gain, and isolation when being scaled down. Therefore, innovative design techniques are required to overcome these limitations [11–20].

In this context, characteristic mode analysis (CMA) emerges as a powerful tool for antenna design. CMA provides insight into the fundamental modes of an antenna structure, enabling designers to optimize the antenna's performance by manipulating these modes. By introducing slots in the patch antenna, it is possible to achieve orthogonal mode separation, thereby reducing cross polarization and enhancing overall performance. Furthermore, enhancing the bandwidth of a miniaturized antenna is crucial for supporting the wide frequency range of 5G. Slot loading in the ground plane is an effective technique to increase the effective current path, thereby broadening the impedance bandwidth. The isolation between MIMO antenna elements is another critical factor. High isolation minimizes mutual coupling, which is essential for maintaining the independent operation of each antenna element. Implementing spiral decoupling (SD) and aperture spiral decoupling (ASD) structures between antenna elements has proven effective in enhancing isolation [21–25].

Mutual coupling, a major issue in MIMO antenna design, leads to performance degradation by causing interference between closely spaced antenna elements. Various techniques have been proposed to address this, including the use of decoupling networks and parasitic elements, which have shown promising results in reducing coupling effects and improving overall antenna performance [2–6]. Additionally, the incorporation of metamaterials and electromagnetic bandgap (EBG)

* Corresponding author: Jyoti C. Kolte (jyotiamolramteke@rediffmail.com).

structures has emerged as an effective strategy for enhancing isolation. Studies in [5] and [9] have demonstrated that EBG structures and split-ring resonators (SRRs) can significantly reduce mutual coupling, thereby improving the isolation between antenna elements [8]. Moreover, the compactness of MIMO antennas is crucial for their integration into modern communication devices. Refs. [25–29] have explored compact MIMO antenna designs specifically for sub-6 GHz 5G applications, utilizing innovative decoupling structures to maintain high performance in a limited space [30]. Likewise, as demonstrated in [31], the application of dual-layer, dual-patch EBG structures has been proven to efficiently suppress surface waves and improve isolation. Notwithstanding these developments, it is still difficult to achieve the required degrees of isolation and cross polarization reduction while keeping a small size. Novel decoupling strategies that provide scalable solutions for multi-band applications, like frequency-selective surfaces and meta-inspired decoupling networks, have been the focus of recent research [32–38].

The novelty of this work lies in the design and development of a highly compact MIMO antenna. By loading novel spiral decoupling (SD) and aperture spiral decoupling (ASD) structures, this work achieves strong isolation between MIMO antenna elements. What makes it novel? By introducing slots into the patch using Characteristics Mode Analysis (CMA), orthogonal mode separation is achieved, hence reducing cross-polarization. Slot loading is incorporated into the ground plane to further boost bandwidth. The resultant MIMO antenna is a promising option for next-generation wireless communication systems due to its notable compactness, high gain, low envelope correlation coefficient (ECC), minimum channel capacity loss, and minimal mutual coupling between parts.

2. GEOMETRY AND WORKING MECHANISM OF PROPOSED ANTENNA

2.1. Overall Antenna Design

Figure 1 illustrates both the top and bottom views of the prototype of the proposed 2×2 MIMO antenna hardware. The antenna has compact dimensions of $30 \times 30 \times 1.6\,\text{mm}^3$ and is constructed using an economical FR4 dielectric material with a relative permittivity ε_r of 4.3 and a loss tangent of 0.025. To minimize the coupling between antenna elements, an aperture spiral decoupling structure is incorporated. The antenna is excited at the fundamental mode of 3.5 GHz, suitable for sub-6 GHz 5G applications, using a 50 Ω SMA connector connected to a microstrip feed line.

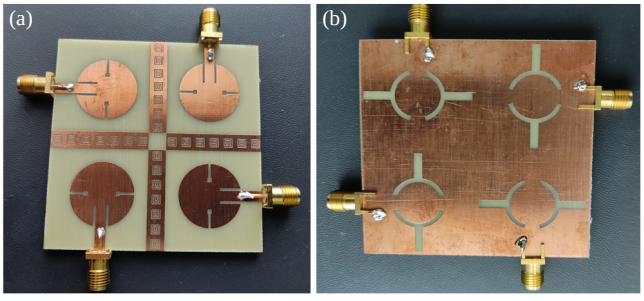

FIGURE 1. The 2×2 MIMO antenna hardware with decoupling structure, (a) front view, (b) back view.

2.2. Cavity Model Method Discussion

Cavity model is applied to study the characteristics of microstrip antennas. This model helps in gaining insights into the resonance modes and performance of these antennas. Cavity model relies on certain assumptions to simplify the analysis. These assumptions often include treating the antenna structure as a resonant cavity, neglecting certain complexities, and assuming that the antenna operates in specific modes. The antenna structure is modeled as a cavity with well-defined boundaries. For microstrip antennas, this could involve representing the substrate, radiating patch, and other elements as part of the cavity as shown in Fig. 2. One degree of freedom parameter (the patch's radius, "R") in a circular patch controls the ordering of resonance modes. The TM^z_{mno} modes resonance frequency of circular patch is given below [21].

$$(f_r)_{mno} = \frac{1}{2\pi\sqrt{\mu\varepsilon}}\left(\frac{\chi'_{mn}}{R}\right) \tag{1}$$

where the orders of resonant frequencies are determined by the roots of the derivative of the Bessel function, denoted by χ'_{mn}. The exact value for the first order, or dominant mode, is 1.8412, and [20] provides the appropriate TM^z_{11o} (dominant mode) frequency.

$$(f_r)_{110} = \frac{1.8412}{2\pi R\sqrt{\mu\varepsilon}} = \frac{1.8412\vartheta_o}{2\pi R\sqrt{\varepsilon_r}} \tag{2}$$

The design parameter "$R = 12.11$ mm" for a circular patch antenna on an FR/4 substrate with a dielectric constant of 4.3 and a loss tangent of 0.025 — which corresponds to the dominant mode of 2400 MHz — is obtained through Equation (2). The cavity dimensions and geometry play a crucial role in determining the resonance frequencies and radiation characteristics. While the cavity model provides valuable insights, it has limitations. It may not accurately represent the behavior of irregularly shaped antennas or those with complex structures. The characteristic mode analysis method is presented in the next section, in which an antenna with an irregularly shaped and complex structure is designed and optimized.

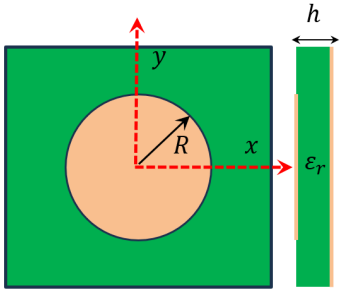

FIGURE 2. Circular patch antenna.

2.3. Brief of Characteristic Mode Theory

Characteristic Mode Theory (CMT) is a powerful analytical framework for understanding and designing antennas. Introduced by Garbacz and Turpin in [39], CMT provides insight into the fundamental resonant behaviors of arbitrary conducting structures. It decomposes the complex current distribution on an antenna into a set of orthogonal modes, each associated with a specific eigenvalue. These modes are intrinsic to the structure and do not depend on the excitation [22–24].

The key advantage of CMT is that it allows designers to visualize and manipulate the resonant modes of an antenna to achieve desired performance characteristics. Each mode has an associated eigenvalue, which indicates how easily the mode can be excited. The eigenvalues are functions of frequency, and their behavior provides valuable information about the resonant characteristics and bandwidth of the antenna.

It is quite difficult to reduce antenna size without sacrificing performance. CMT facilitates this approach by offering a thorough comprehension of the structure's resonance behavior and current distribution. Miniaturization can be accomplished without sacrificing performance by tailoring the antenna's physical dimensions and shape to its characteristic modes. For instance, adding reactive parts to the antenna or carefully positioning slots can help it get smaller without sacrificing its radiation properties and resonant frequencies. In antenna designs, CMT can be used to lessen cross polarization. In order to accomplish orthogonal mode separation, designers can alter the antenna shape by examining the orthogonal modes and their corresponding current distributions. This improves antenna performance by lowering undesired cross-polarized radiation, especially in MIMO systems where polarization diversity is crucial.

1. Characteristic Equation: The fundamental equation in Characteristic Mode Theory (CMT) is the characteristic equation which is used to solve for the characteristic modes of a conducting structure. This equation is expressed as [22–24]:

$$ZI_n = \lambda_n R' I_n \tag{3}$$

where Z is the impedance matrix, R' the resistance matrix, I_n the current distribution of the nth mode, and λ_n the eigenvalue associated with the nth mode.

2. Eigenvalue: The eigenvalue λ_n is an important parameter in CMT, providing information about the mode's radiation efficiency. For practical antenna design, the real part of the eigenvalue λ_n is of interest, indicating how easily a mode can be excited [22–24].

3. Modal Significance: Modal significance (MS) is a measure of how significant a mode is at a particular frequency and is given by [22, 23]:

$$\text{MS} = \frac{1}{|1 + je_n|} \tag{4}$$

4. Characteristic Angle: Characteristic angle provides insight into the behavior of each mode across the frequency range [22–24].

$$\text{CA} = 180^\circ - \tan^{-1}(\lambda_n) \tag{5}$$

Characteristic angle (CA) indicates the resonance condition of a mode. When CA is close to 180° (or π), the mode is at resonance. The characteristic angle reflects the reactive nature of the mode. If CA is close to 90° (or $\pi/2$ radians), the mode is predominantly reactive (capacitive or inductive) and does not contribute significantly to radiation. Modes with CA around 0° or 180° are more radiative. When performing CMA in Computer Simulation Technology (CST), the antenna is usually assumed to be lossless and modeled with Perfect Electric Conductor (PEC) materials. No external excitations like ports are used, as CMA analyzes the natural resonant modes without sources. Open or radiation boundaries are needed for radiating structures. A fine mesh is required to accurately resolve current distributions. After simulation, key results such as eigenvalues, modal significance, modal currents, and radiation patterns help identify the dominant resonant modes and understand the antenna's radiation behavior.

2.4. Orthogonal Mode Separation and Miniaturization of Antenna Using CMA

Figure 3 illustrates the antenna miniaturization strategy. In Fig. 3(a), Antenna-1 represents the conventional circular microstrip patch antenna configuration, whereas Fig. 3(b) shows Antenna-2, the miniaturized variant achieved by introducing perturbations such as inner ring cuts ($L1, L2$) and slot widths ($W1, W2$), effectively reducing the resonant dimension without significantly degrading radiation performance.

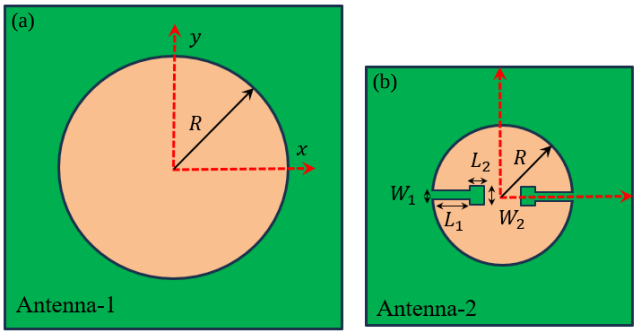

FIGURE 3. Antenna miniaturization steps: (a) Antenna-1 (conventional circular patch antenna), and (b) Antenna-2 (miniaturized antenna).

Figure 4 presents the modal significance (MS) plots derived from the Characteristic Mode Analysis (CMA) for Antenna-1 at varying radius (R) values. The MS curves provide a quantitative measure of how strongly each mode is excited around its resonant frequency, indicating which modes predominantly contribute to radiation. As R increases, the primary resonance shifts to lower frequencies, and the modal behavior evolves, affecting bandwidth and radiation efficiency. This analysis guides the geometric optimization for efficient miniaturization while maintaining desirable electromagnetic performance.

Figure 5 illustrates the eigenvalue plot for the circular patch antenna. Eigenvalues are crucial in understanding the resonant

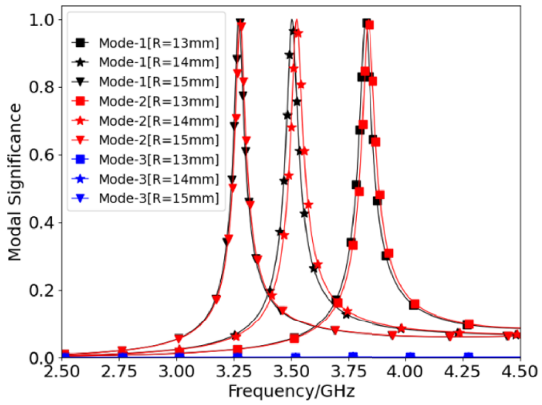

FIGURE 4. Modal significant plots for Antenna-1 with different R values.

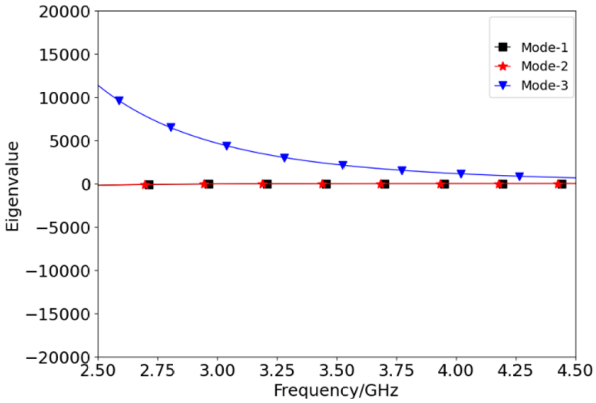

FIGURE 5. Eigenvalue plots for Antenna-1.

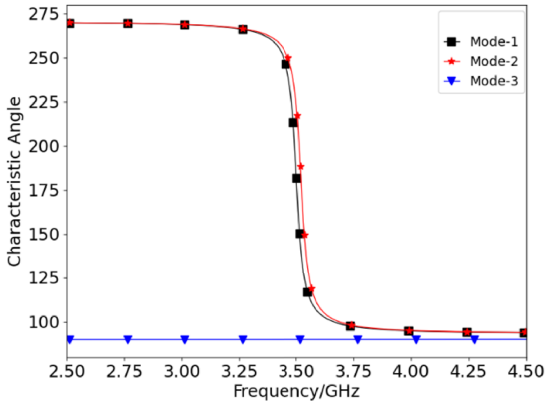

FIGURE 6. Characteristic angle plots for Antenna-1.

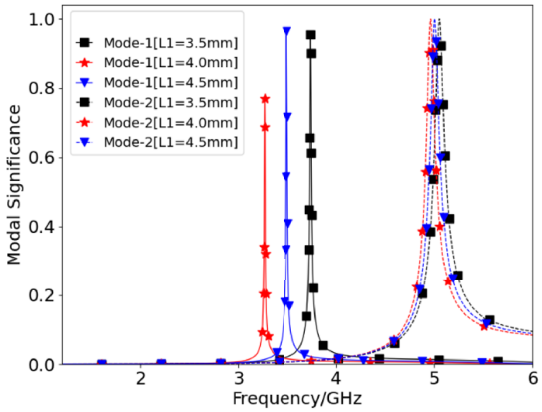

FIGURE 7. Modal significant plots for Antenna-2 with different $L1$ value of slots.

behavior of the antenna modes. For Modes 1 and 2, the eigenvalues exhibit overlap to zero line at their respective resonance frequencies, indicating strong resonance behavior. These dips correspond to the frequencies where the antenna radiates efficiently. In contrast, Mode 3 shows a relatively positive eigenvalue value, signifying stored magnetic energy not associated with radiation.

Figure 6 shows the characteristic angle plots for Antenna-1 across a frequency range of 2.5 GHz to 4.5 GHz, highlighting the behavior of three different modes (Mode-1, Mode-2, and Mode-3). Mode-1 and Mode-2 exhibit a significant change in characteristic angle between 3.25 GHz and 3.75 GHz, indicating the antenna's resonant frequency range and for efficient radiation and impedance matching in this bandwidth. Mode-3, however, maintains a constant characteristic angle about 100 degrees across the entire frequency range, suggesting minimal excitation or no significance for radiation.

2.5. CMA Analysis of Antenna-2

To miniaturize the circular conventional antenna, the two symmetrical slots are loaded in patch in horizontal direction. The conductive length at 3.5 GHz is increased by loading the slots, resulting in resonance frequency shifted in lower side as shown in Fig. 7 with different values of $L1$ slot parameters. In this plot increasing the $L1$ values Mode-1 is more sensitive than Mode-2, and Mode-1 is shifted in lower side due to a slot loaded in horizontal direction. If slot is loaded in vertical direction, Mode-2 frequency is more sensitive than Mode-1. So by loading slot, we can separate Mode-1 and Mode-2 with large frequency gap, resulting in improvement in co- and cross-polarizations, which will be discussed in the next section.

Figure 7 illustrates the impact of varying parameter $L1$, which represents the length of the symmetrical slots loaded into the patch of a miniaturized circular conventional antenna. The purpose of incorporating these slots is to reduce the size of the antenna while maintaining its performance. The plot in Fig. 7 displays the resonance frequencies of different modes of the antenna as the parameter $L1$ changes. At a frequency of 3.5 GHz, the conductive length is increased due to the slots loaded into the patch. This increase in conductive length causes a shift in the resonance frequency towards the lower end. One notable observation from the plot is that as the value of $L1$ increases, Mode-1 experiences a more significant shift in its resonance frequency than Mode-2. This behavior is attributed to the horizontal loading of the slots. When the slots are loaded horizontally, Mode-1 is more sensitive to changes in the slot parameters than Mode-2.

On the other hand, Mode-2 would be more sensitive than Mode-1 if the slots were loaded vertically. This implies that a key factor in identifying which mode is more impacted by

modifications to the slot characteristics is the orientation of the loaded slots. Mode-1 and Mode-2 with a large frequency gap can be distinguished by varying the loaded slots' properties, such as length ($L1$). The antenna's co- and cross-polarization properties are improved as a result of this separation.

Figure 8 illustrates the modal significance plot of Antenna-2, showcasing the impact of varying parameter $L2$, which represents the length of a slot in the antenna design. This slot is presumably employed to further optimize the antenna's performance. The plot demonstrates that as the length of the slot ($L2$) increases, Mode-1 becomes increasingly sensitive to changes in this parameter. Conversely, Mode-2 shows little to no sensitivity to variations in the length of the slot.

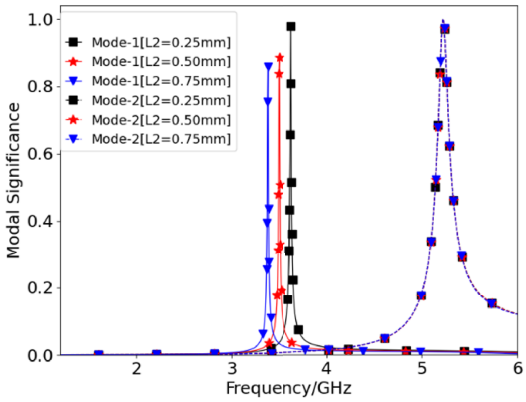

FIGURE 8. Modal significant plots for Antenna-2 with different $L2$ value of slots.

This behavior suggests that the resonance frequency of Mode-1 can be efficiently controlled by varying the slot's length ($L2$) without appreciably altering the resonance frequency of Mode-2. Because it enables more accurate tuning of certain modes without unintentionally altering others, this decoupling of sensitivity between the two modes is a desired feature in antenna design. Practically speaking, this means that the antenna designer can adjust the Mode-1 resonance frequency to satisfy specific design specifications or performance goals without unintentionally shifting the Mode-2 resonance frequency. In a variety of applications, this degree of control over specific modes can result in improved antenna performance and usefulness.

Figure 9 provides a visual representation of the surface current distribution for both Antenna-1 and Antenna-2, highlighting how miniaturization and orthogonal mode separation are achieved through the design modifications. For Antenna-1, the surface current distributions of Mode-1 and Mode-2 are depicted as orthogonal to each other at the same frequency. This orthogonal arrangement suggests that the two modes are independent of each other and do not interfere. The surface current arrows for both modes exhibit a pure $\lambda_1/2$ current distribution, indicating a dominant mode behavior for each mode. This signifies that Antenna-1 operates with distinct and well-defined modes, contributing to its overall performance.

In contrast, Antenna-2 features the incorporation of loaded slots in the horizontal direction. This modification alters the surface current distribution, particularly for Mode-1.

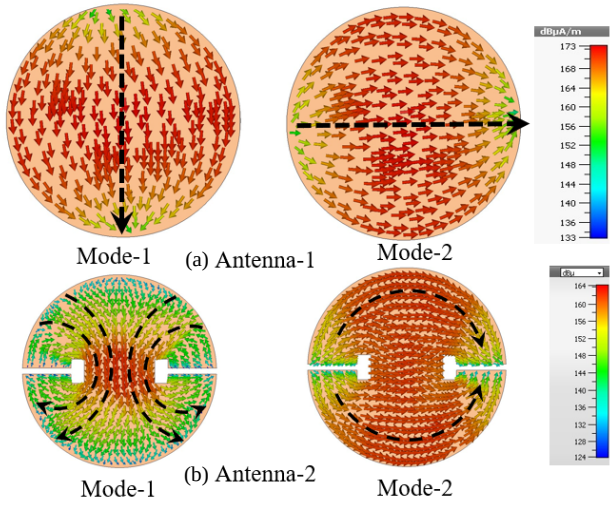

FIGURE 9. Surface current distribution on antennas at 3.5 GHz, (a) Antenna-1 and (b) Antenna-2.

The surface current distribution for Mode-1 becomes more concentrated and exhibits a longer conductive path for the $\lambda_1/2$ current distribution than that of Antenna-1, indicating improved current flow and potential radiation efficiency. This increased sensitivity and enhanced conductive path indicate that Mode-1 is more influenced by the design changes introduced by the loaded slots in Antenna-2. As a result of these modifications, the resonance frequency of Mode-1 in Antenna-2 is effectively reduced without significantly affecting the resonance frequency of Mode-2. This decoupling of the resonance frequencies of the two modes allows for independent control over Mode-1, enabling miniaturization of the antenna while maintaining desired performance characteristics.

2.6. Full Wave Analysis of Antenna-1 and Antenna-2

Figure 10 presents discussion of the antenna geometry of Antenna-1 (conventional antenna) and Antenna-2 (miniaturized antenna) using a 50-ohm microstrip feed line, conducted in the time domain with CST Studio Suite. Fig. 11 shows the scattering parameters of Antenna-1 and Antenna-2. The bandwidth of Antenna-1 is greater than that of Antenna-2 at the same resonance frequency due to impedance matching in the narrow band. Therefore, further modifications are

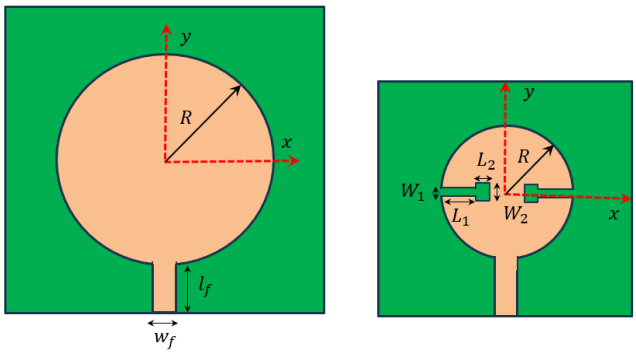

FIGURE 10. The antenna geometry for Antenna-1 and Antenna-2 using microstrip feed line.

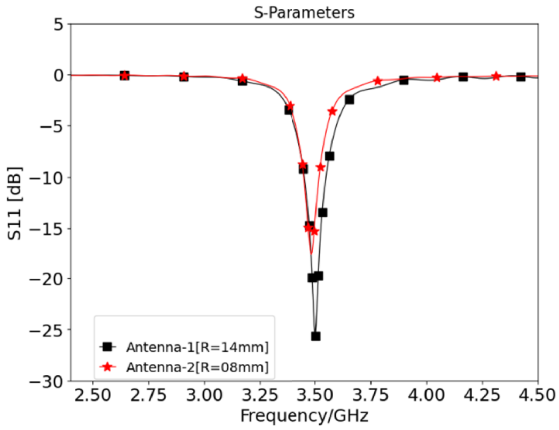

FIGURE 11. S_{11} plots of Antenna-1 and Antenna-2.

TABLE 1. Proposed antenna parameters.

Parameters	Values (mm)	Parameters	Values (mm)
L	30	L_3	7
h	1.6	W_1	0.50
L_1	4	W_2	1.10
L_2	1.10	W_3	1
w_g	0.50	l_g	5.87
w_f	3	l_f	6.13
R	8.9	θ	144°

needed to enhance the bandwidth to meet the sub-6 GHz 5G requirements.

2.7. Bandwidth Enhancement of Proposed Antenna

Impedance matching with slot loading in the antenna ground significantly enhances the bandwidth of an antenna by altering its impedance characteristics. Introducing a slot in the ground plane, whether it is a simple slot or a more complex dumbbell shape, creates additional reactive components — inductance and capacitance — whose resonance frequency can be tuned by adjusting the shape and dimensions. This tuning allows for better impedance matching over a wider frequency range, as the inductive and capacitive effects can offset the natural impedance variations of the antenna. The careful design and optimization of slots are essential to maximizing these benefits and achieving the desired performance enhancements in modern communication systems. This bandwidth enhancement is primarily attributed to the implementation of slot loading in the ground plane, which plays a critical role in impedance matching. The incorporation of slots — such as dumbbell-shaped or optimized rectangular slots — introduces distributed inductive and capacitive elements that modify the antenna's input impedance. These reactive elements enable tuning of the resonance behavior, effectively broadening the impedance bandwidth by mitigating mismatch across a wider frequency span. Through precise design and parametric optimization of the slot geometry and positioning, the antenna achieves improved return loss characteristics and maintains stable radiation performance over the entire operating band.

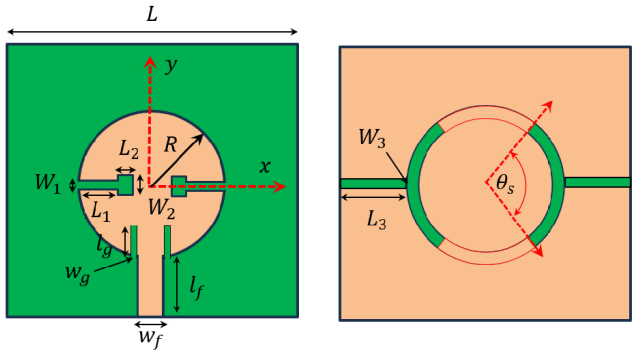

FIGURE 12. Slots loaded proposed antenna.

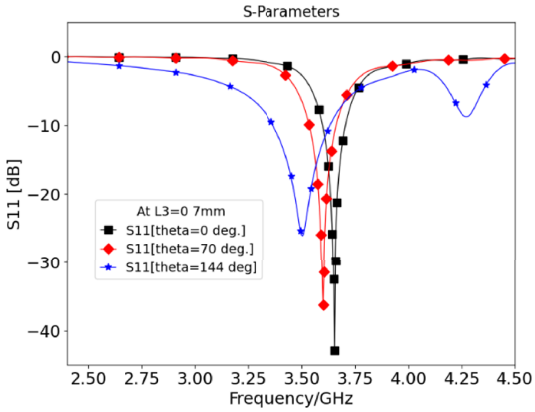

FIGURE 13. S_{11} plots of proposed antenna with varying slot theta values.

Figure 12 presents the proposed antenna design aimed at enhancing bandwidth through slot loading in the antenna ground. This design incorporates two symmetrical slots in the antenna ground, with tuning parameters including dimensions L_3, W_3, and θ. The corresponding design parameters of proposed antenna are mentioned in Table 1. Fig. 13 illustrates the S_{11} parameters while maintaining constant values for L_3 and W_3, and varying the angle θ from 0° to 144°. It is observed that as the θ parameter is varied, the antenna's bandwidth increases significantly, achieving a large bandwidth match near 50 ohms due to the introduction of additional reactive components. Moreover, the structure experiences further miniaturization, attributed to the increased conducting path in the ground plane. Fig. 14 illustrates the variation of S_{11} with slot parameter $L3$. In this plot, it is observed that increasing $L3$ results in a rapid decrease in resonance frequency without significantly enhancing bandwidth. Instead, the primary effect appears to be an increase in the conducting path for the fundamental mode for miniaturization. Therefore, it is concluded that for bandwidth enhancement, parameter θ is more effective. By adjusting θ, we can effectively broaden the antenna's bandwidth.

The proposed antenna's surface current distribution, analyzed comprehensively, reveals that the fundamental mode is excited by a 50 Ω microstrip feed line, as depicted in Fig. 15. The slots loaded in the patch part contribute to the antenna's

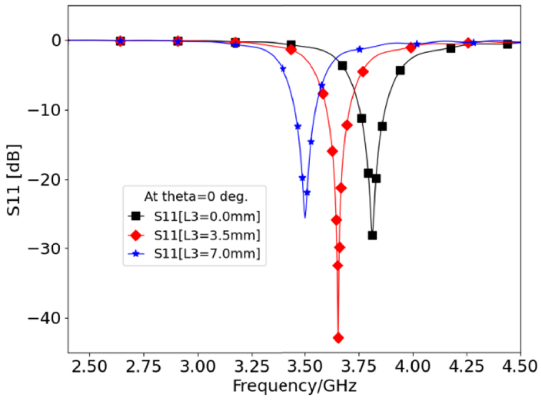

FIGURE 14. S_{11} plots of proposed antenna with varying slot L_3 values.

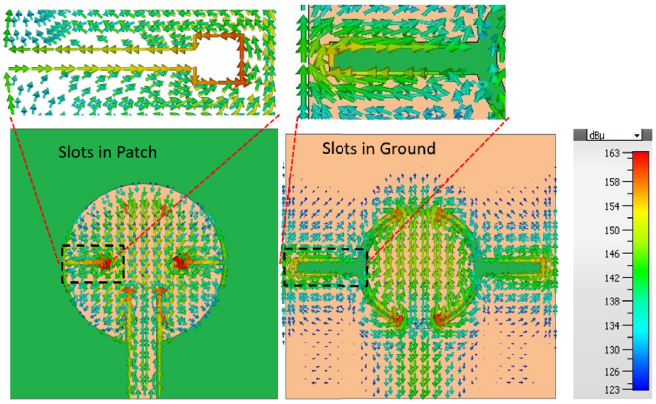

FIGURE 15. The surface current distribution of proposed antenna with full wave analysis using microstrip feed line.

miniaturization by increasing the conducting path of the surface current, primarily for the fundamental mode. Simultaneously, the slots loaded in the antenna ground play a crucial role in bandwidth enhancement by introducing additional reactive components, facilitating a wide range of 50 Ω impedance matching. Furthermore, these ground slots also augment the surface current path, aiding in further miniaturization of the antenna. The slots on the patch mainly modify the surface current distribution of Mode-1 by increasing the effective current path, lowering the resonant frequency, and allowing finer control of the fundamental mode. On the other hand, the ground-loaded slots strongly influence Mode-2 and higher-order modes by introducing additional coupling paths and altering the current return flow, which enhances the excitation and separation of these modes. Together, as seen in Figs. 9 and 15, the combination of patch and ground slots improves mode control, enables better tuning of multiple resonances, and enhances bandwidth, as reflected in the S_{11} results of Fig. 14.

Figure 16 demonstrates the exceptional performance of the proposed antenna, with both total and radiation efficiencies consistently between 50 and 70% in frequency 3.4–3.6 GHz. This achievement is attributed to the antenna's simple structure and low conduction loss, highlighting its effectiveness in converting input power into radiated electromagnetic energy.

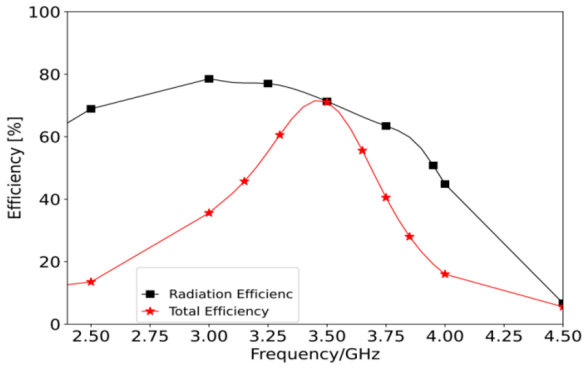

FIGURE 16. The total and radiation efficiency of proposed antenna.

In Fig. 17, the co- and cross-polarization characteristics of the proposed antenna are depicted in both the E-plane (electric field plane) and H-plane (magnetic field plane) at a frequency of 3.5 GHz. The graph illustrates that the proposed antenna exhibits favorable co- and cross-polarization behavior. Co-polarization refers to the polarization of the radiated electromagnetic waves being parallel to the orientation of the transmitting antenna's electric field. Cross-polarization, on the other hand, occurs when the polarization of the radiated waves is perpendicular to the orientation of the transmitting antenna's electric field. The analysis indicates that the proposed antenna demonstrates good co- and cross-polarization characteristics, which is essential for efficient and reliable communication systems. The reduction of cross-polarization, particularly in both E and H polarizations, is achieved through mode separation techniques as discussed in the CMA analysis of Antenna-2.

In this case, the analysis likely reveals that while the fundamental mode is primarily responsible for radiation, there are contributions from orthogonal modes as well. Orthogonal modes, being different from the primary mode, can introduce cross-polarization components into the antenna's radiation pattern. To mitigate the effects of cross-polarization, mode separation techniques are employed. By creating a frequency gap between the fundamental mode and orthogonal modes, the effectiveness of the latter in contribution to radiation is reduced. This separation effectively minimizes the cross-polarization, ensuring that the antenna maintains good polarization characteristics.

2.8. Antenna Hardware Testing

Figures 18 and 19 provide a comprehensive validation of the proposed antenna's performance. The measured S_{11} parameters and gain closely match the simulated results, with minor variations due to fabrication and instrumentation uncertainties. These comparisons underscore the robustness of the antenna design and its effective implementation in practical applications.

2.9. Design MIMO Antenna

In Fig. 20, the 2 × 1 MIMO antenna is depicted, showcasing both the front and back views. This antenna configuration consists of two individual antenna elements arranged in a 2 × 1 setup, meaning that there are two transmitting/receiving

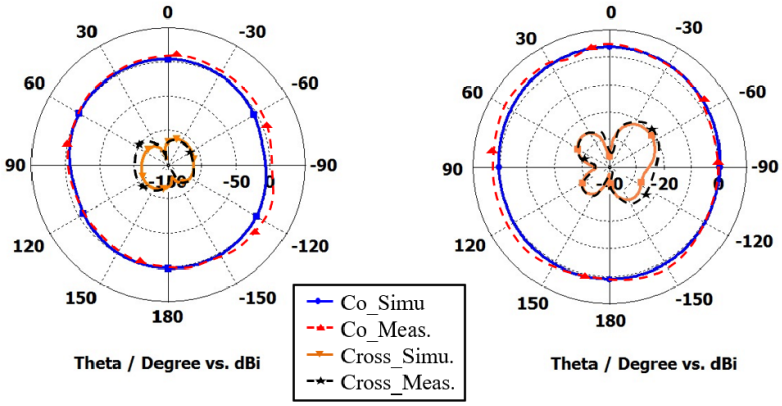

FIGURE 17. The co- and cross-polarizations of proposed antenna in E and H planes at 3.5 GHz.

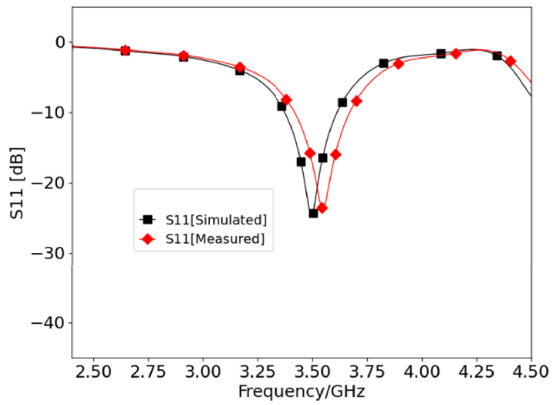

FIGURE 18. The comparison between simulated and measured S_{11} plots.

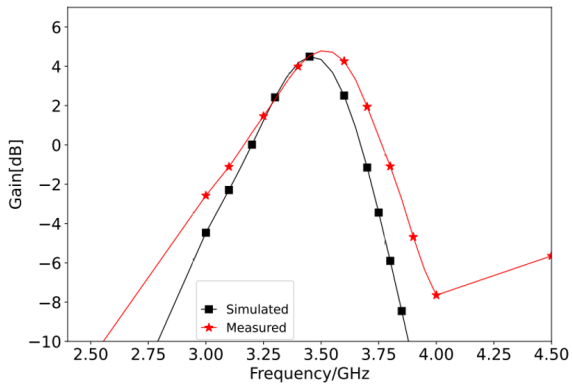

FIGURE 19. The comparison between simulated and measured gain plots.

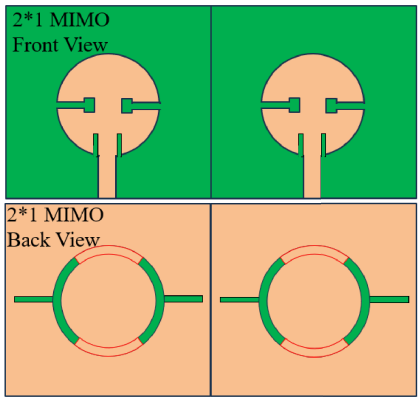

FIGURE 20. The 2×1 MIMO antenna, front and back views.

elements positioned in a linear array. The figure emphasizes that the 2×1 MIMO antenna does not include any decoupling structures. Decoupling structures are typically used in MIMO systems to minimize the mutual coupling between antenna elements, which can degrade performance by causing interference and reducing isolation. The analysis of scattering parameters, particularly S-parameters, is crucial for understanding the electromagnetic behavior of the MIMO antenna. S-parameters describe how radio frequency (RF) signals behave in a network, indicating how much power is reflected, transmitted, and coupled between ports (antenna elements).

In the analysis, the performance degradation of the MIMO antenna due to near-field electromagnetic coupling is tested. Electromagnetic coupling occurs when the fields from one antenna element interact with another, leading to interference and reduced isolation. This coupling can significantly affect the performance of the MIMO system, causing reduced diversity gain, increased correlation between signals, and impedance mismatch. Reduced diversity gain occurs as high coupling diminishes the independence of multiple signal paths, crucial for enhancing data rates and reliability. Increased correlation due to high coupling undermines MIMO performance by reducing signal independence. Impedance mismatch results from coupling altering the input impedance of antenna elements, leading to higher reflection coefficients (S_{11}, S_{22}) and poorer impedance matching. The absence of a decoupling structure in the depicted MIMO antenna necessitates a careful design to mitigate these negative effects. Techniques such as optimizing the physical separation between elements, using different polarization schemes, or implementing specific antenna geometries can help reduce coupling and maintain good MIMO performance.

Figure 21(a) shows the spiral decoupling (SD) structure loaded onto a microstrip line designed on an FR4 substrate with a height of 2.4 mm. This structure is designed to minimize mutual coupling between two radiating elements, effectively acting as an isolator at 3.5 GHz. The decoupling structure sig-

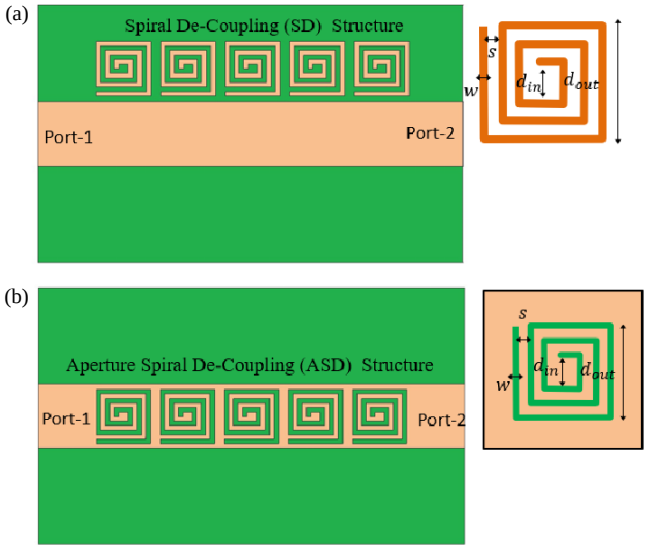

FIGURE 21. Decoupling structure loaded in microstrip transmission line. (a) Spiral decoupling structure. (b) Aperture spiral decoupling coupling structure. [$d_{in} = 0.85$ mm, $d_{out} = 2.5$ mm, $s = 0.25$ mm, $w = 0.25$ mm].

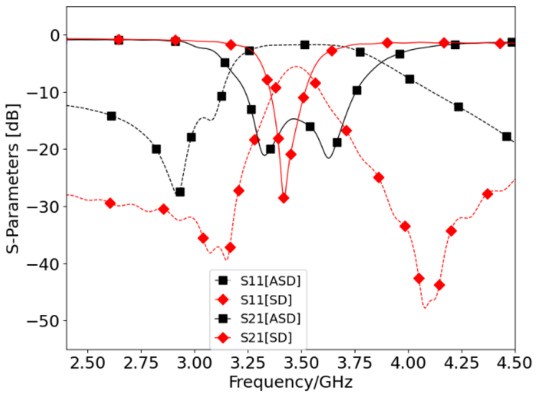

FIGURE 22. S-parameters of decoupling structure loaded in microstrip transmission line. (a) Spiral decoupling structure. (b) De-aperture spiral coupling structure.

nificantly reduces interference between the antenna elements, thereby enhancing the overall performance of the MIMO system. The S-parameters of the SD structure are presented in Fig. 22, where the notch frequency, indicated by the S_{21} transmission coefficient, reaches approximately -30 dB. However, the SD structure exhibits a narrow bandwidth, which is insufficient to cover the entire sub-6 GHz band (3.4–3.6 GHz) required for 5G applications.

To address this limitation, an aperture spiral decoupling (ASD) structure is introduced, as shown in Fig. 21(b). The ASD structure, also loaded in a microstrip line, provides a broader bandwidth suitable for decoupling electromagnetic signals within the 3.4 to 3.6 GHz frequency range, covering the sub-6 GHz band essential for 5G applications. The corresponding S-parameters for the ASD structure are also presented in Fig. 22, demonstrating its enhanced performance in providing isolation over a wider frequency range than the narrower bandwidth of the SD structure.

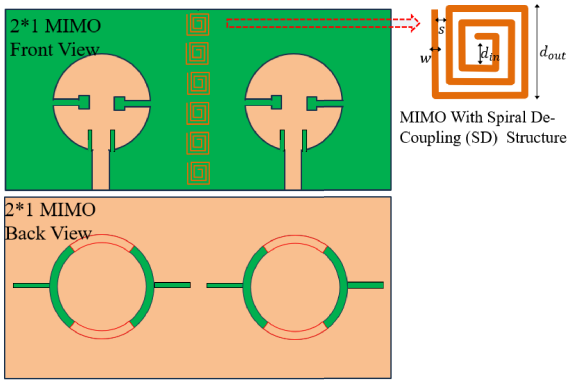

FIGURE 23. The 2×1 MIMO antenna with spiral decoupling structure, front and back view.

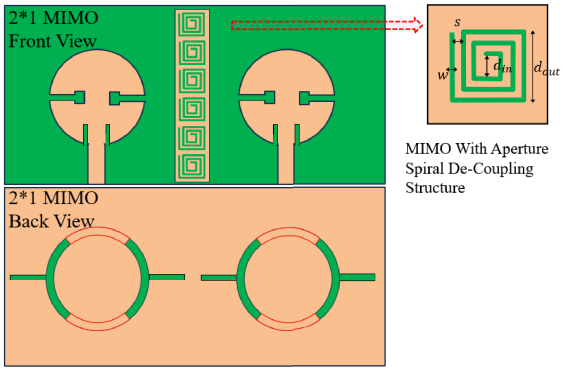

FIGURE 24. The 2×1 MIMO antenna with aperture spiral decoupling structure, front and back view.

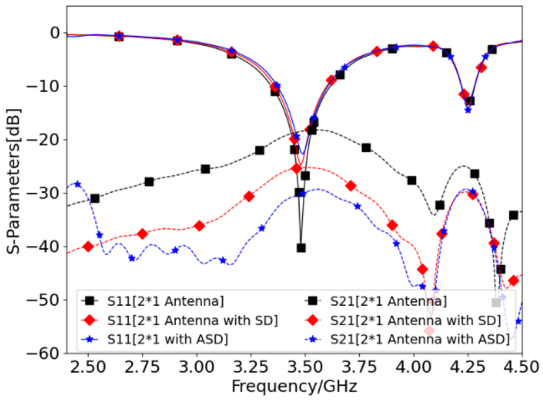

FIGURE 25. S-parameters of MIMO antenna with decoupling structure. (a) With Spiral decoupling structure, (b) with de-aperture spiral coupling structure.

The 2×1 MIMO antenna's performance with both spiral decoupling (SD) and aperture spiral decoupling (ASD) structures is analyzed to assess their effectiveness in minimizing mutual coupling. Fig. 23 displays the 2×1 MIMO antenna integrated with the spiral decoupling structure, while Fig. 24 shows the 2×1 MIMO antenna with the aperture spiral decoupling structure. The corresponding S-parameters of the MIMO antennas with these decoupling structures are illustrated in Fig. 25. The S_{21} parameter specifically highlights the mutual coupling

between the antenna elements. The analysis reveals that the MIMO antenna with the ASD structure demonstrates better isolation than the spiral decoupling (SD) structure. This is evident from the S_{21} parameters, where the ASD structure exhibits lower mutual coupling between antenna elements, indicating superior performance in mitigating interference.

This improved isolation is further analyzed through the electric field distribution shown in Figs. 26(a)–(c). Fig. 26(a) illustrates the electric field distribution for a MIMO antenna without any decoupling structure, revealing significant coupling between antenna elements, which corresponds to the higher mutual coupling observed in Fig. 25. Fig. 26(b) depicts the MIMO antenna with the spiral decoupling structure, showing a reduction in electric field coupling compared to the antenna without any decoupling. Finally, Fig. 26(c) presents the MIMO antenna with the aperture spiral decoupling structure, where the electric field isolation is further enhanced, demonstrating minimal coupling between antenna elements.

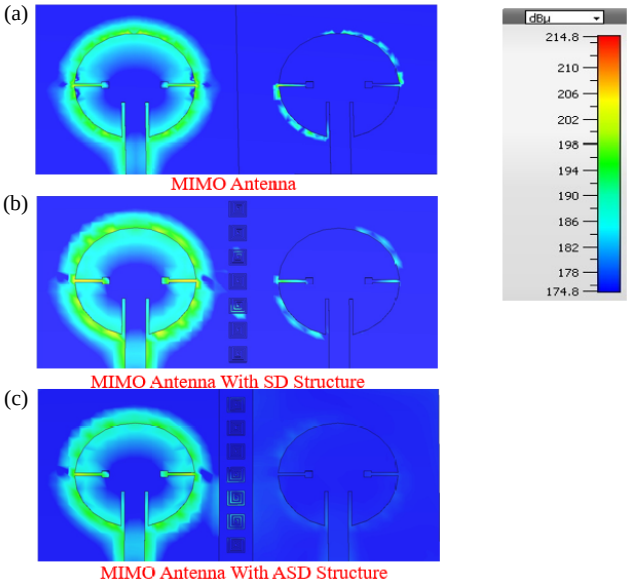

FIGURE 26. Electric field distribution of MIMO antenna. (a) MIMO without decoupling structure, (b) MIMO with spiral decoupling structure, and (c) MIMO with de-aperture spiral coupling structure.

2.10. Diversity Performance of MIMO Antenna

Figure 27 illustrates the detailed structure of the proposed 2×2 MIMO antenna with an ASD structure designed for sub-6 GHz 5G applications. The overall geometry of this MIMO antenna is compact, measuring $60 \times 60 \times 1.6\,\text{mm}^3$. Each antenna element within the MIMO system is connected via a $50\,\Omega$ microstrip feed line, oriented differently to optimize performance and minimize mutual coupling. The scattering parameters of this MIMO antenna, shown in Fig. 28, include S_{11}, S_{22}, S_{33}, and S_{44}, which represent the reflection coefficients for each of the four ports, and S_{12}, S_{13}, S_{14}, S_{32}, S_{42}, and S_{43}, which represent the mutual coupling parameters between all port pairs. These parameters indicate that the antenna resonates at 3.5 GHz, effectively covering the 3.4 to 3.6 GHz range required for sub-6 GHz 5G bandwidth. The corresponding 3D radiation patterns for each antenna element are depicted in Fig. 29. The antenna elements exhibit consistent directional radiation with good gain and beam symmetry, supporting reliable MIMO performance. Additionally, a slight beam tilt is observed, which results from asymmetry in the antenna layout and mutual coupling effects. This tilt remains within acceptable limits and can even be advantageous in enhancing coverage in certain deployment scenarios, demonstrating the effective isolation of the MIMO system, which is below -25 dB at 3.5 GHz. This high level of isolation highlights the effectiveness of the aperture spiral decoupling structure in minimizing interference and enhancing the overall performance of the 2×2 MIMO antenna for 5G applications.

Isolation and radiation patterns are not the only factors to consider when evaluating the performance of a MIMO antenna.

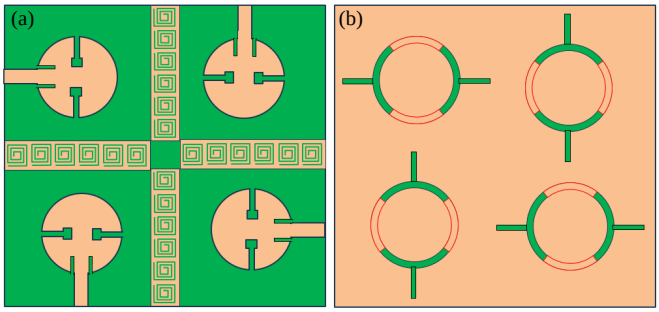

FIGURE 27. The 2×2 MIMO antenna, (a) front view, (b) back view.

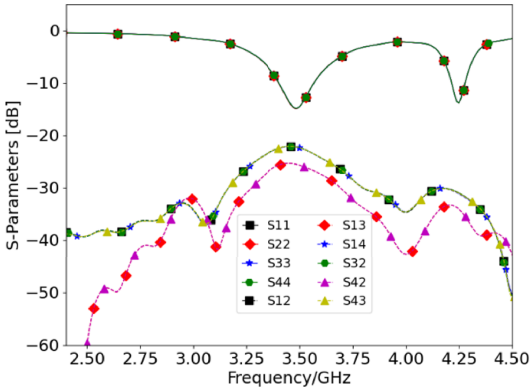

FIGURE 28. The scattering parameters of 2×2 MIMO antenna.

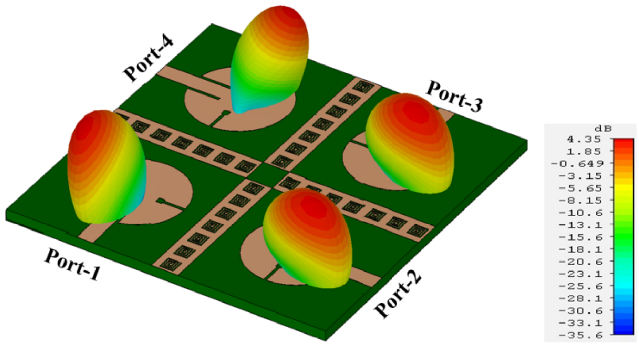

FIGURE 29. The 3D radiation pattern of 2×2 MIMO antenna at 3.5 GHz.

In multipath situations, diversity performance is crucial for increasing signal dependability and throughput, and it significantly affects MIMO antenna performance. Diversity Gain (DG) and Envelope Correlation Coefficients (ECC) are used to characterize the performance of diversity. A low ECC suggests that the signals are mainly independent, which is ideal for efficient MIMO operation. ECC is a measure of the correlation between the signals received by the antenna elements. For uncorrelated transmissions, DG is ideally around the theoretical maximum of 10 dB and measures the improvement in signal quality brought about by variety. To provide a thorough assessment of the MIMO antenna's diversity performance and make sure that it satisfies the requirements of 5G applications, we examine these crucial factors in this section.

2.10.1. Envelope Correlation Coefficients (ECCs)

The performance of an antenna is reduced by a high ECC value because it causes significant correlation and little isolation. Additionally, ECC illustrates how the total S-parameters of the designed MIMO antennas interact with one another. Different methods, such as employing the received signal envelope, S-parameter, or far-field radiation for the estimate of complex cross correlation, can be used to find the ECC. As can be seen in Equations (6) and (7) of this work, ECC is calculated using both the S-parameter and far-field radiation patterns methods [4, 23]. ECC from radiation patterns data requires a tedious integral computation. Fig. 30 illustrates the ECC characteristic of 2×2 MIMO systems and shows that for scattering parameters, the ECCs are very low (i.e., 0.001) throughout the entire bandwidth.

$$\rho_{12} = \frac{\left|\iint_0^{4\pi}\left[\vec{F}_1(\theta,\emptyset)X\vec{F}_2(\theta,\emptyset)d\Omega\right]\right|^2}{\iint_0^{4\pi}\left|\vec{F}_1(\theta,\emptyset)\right|^2 d\Omega \iint_0^{4\pi}\left|\vec{F}_2(\theta,\emptyset)\right|^2 d\Omega} \tag{6}$$

where ρ_{12} represents the ECC. $\vec{F}_1(\theta,\emptyset)$ and $\vec{F}_2(\theta,\emptyset)$ are the far-field radiation patterns for port-1 and port-2 of this MIMO antenna.

$$\text{ECC} = \frac{\left|S_{11}\times S_{12} + S_{21}\times S_{22}\right|^2}{\left(1-\left|S_{11}\right|^2-\left|S_{21}\right|^2\right)\left(1-\left|S_{22}\right|^2-\left|S_{12}\right|^2\right)} \tag{7}$$

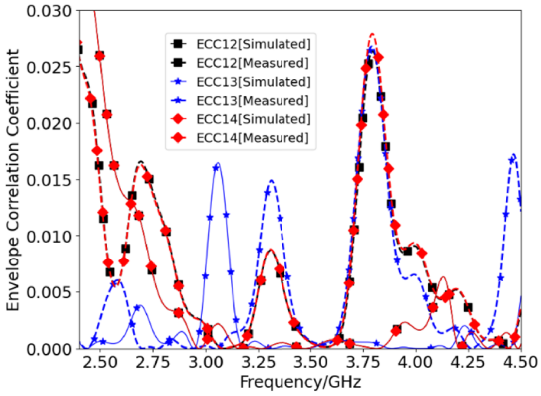

FIGURE 30. The ECC for 2×2 MIMO antenna.

The antenna's reflection and transmission coefficients are S_{11}/S_{22} and S_{21}/S_{12}, respectively.

The low ECC values indicate excellent diversity performance, ensuring minimal signal correlation and effective isolation between the antenna elements. This low correlation is crucial for MIMO systems, as it allows for better exploitation of multipath environments, leading to improved signal reliability and higher data throughput. The comprehensive analysis of ECC using both S-parameter and far-field radiation patterns confirms that the proposed MIMO antenna design effectively meets the requirements for high-performance 5G applications.

2.10.2. Diversity Gain

Diversity Gain (DG) refers to the improvement in signal-to-noise ratio (SNR) that a MIMO system achieves compared to a single antenna. It quantifies the effectiveness of the MIMO system in exploiting spatial diversity to enhance signal quality and reliability. In [20], DG is calculated using Equation (8), and the results are plotted in Fig. 31. The computed DG values from both simulated and measured ECCs are consistently close to the theoretical maximum of 10 dB. This indicates that the MIMO antenna system is highly effective in leveraging diversity to improve signal performance. The near 10 dB DG value underscores the antenna's capability to provide robust performance in multipath environments, making it well suited for high-demand 5G applications. For a MIMO antenna, the DG can be approximated by [20]:

$$\text{DG} \approx 10\sqrt{1-(\text{ECC})^2} \tag{8}$$

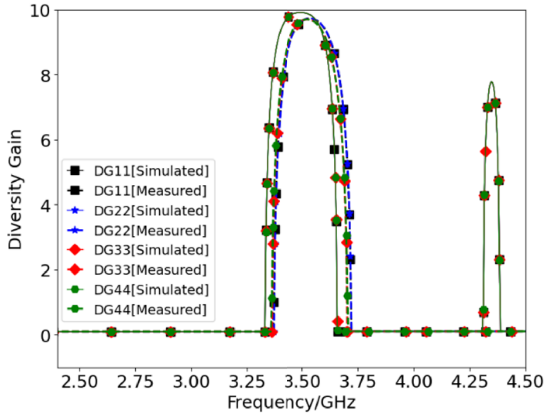

FIGURE 31. The diversity plot of 2×2 MIMO antenna.

Table 2 provides a comprehensive performance comparison between our proposed antenna and various multi-band antennas from prior studies. Our antenna distinguishes itself with a low-profile and straightforward design approach, exhibiting broadside radiation patterns across all bands. This makes it a compelling choice for a wide range of wireless communication applications, delivering enhanced performance.

2.11. MIMO Antenna Hardware Fabrication and Testing

The experimental validation of the proposed antenna was carried out using standard measurement procedures. The antenna

TABLE 2. Relative work comparison table with proposed antenna.

Ref.	Size (λ_o)	Frequency Bands (GHz)	Methods	Gain (dBi)	Port Isolation	ECC
[26]	$0.43 * 0.43$	3–12	Asymptote-shaped structure	2–2.5	> 16.5	< 0.02
[27]	$0.7 * 0.53$	-	Grounded stub	-	50	-
[28]	$0.32 * 0.37$	28	DGS+Partial ground	6.5	> 30	< 0.18
[29]	$0.28 * 0.28$	2.42–7.45	Using stub	2.5	> 12	0.004
[30]	$0.45 * 0.15$	3.3–3.6, 4.4–5	Multiple orthogonal modes	5	> 24	-
[31]	$0.09 * 0.43$	3.4–3.6, 4.8–5	Stop band filter	4	> 12	
[32]	$0.23 * 0.06$	3.37–3.61, 4.9–5.1	Slot in ground	3.9	> 14	0.05
[33]	$0.84 * 0.48$	3.7–4.3	Slot coupling	4.1	> 25	0.1
[34]	0.69*0.52	5.2	Microstrip line	-	> 26	0.05
[35]	$0.70 * 0.44$	3.3–7.8	Fence-shaped decoupling structure	-	> 20	< 0.05
[36]	$1.11 * 1.11$	3.1–11.11	Parasitic de-coupler	6.35	20	0.001
[37]	$1.29 * 0.64$	1.92–2.51	Decoupling element	6.28	> 15	0.0037
This work	$\mathbf{0.32 * 0.32}$	**3.4–3.6**	**Aperture spiral decoupling structures**	**5.1**	$\mathbf{> 32}$	**0.015**

was fabricated on an FR4 substrate with a thickness of 1.6 mm through the chemical etching method, and a 50 Ω SMA connector was used for interfacing with the test equipment. For S-parameter measurements, an Anritsu MS2037C Vector Network Analyzer (VNA) was used, as shown in Fig. 32(a), covering the relevant frequency band. The radiation characteristics, including gain, directivity, and diversity gain (DG), were measured in a fully shielded anechoic chamber to ensure an interference-free environment. As illustrated in Fig. 32(b), the setup allowed for accurate far-field measurements by eliminating external noise and reflections. These measurements confirm the antenna's simulated performance and demonstrate its effectiveness for sub-6 GHz 5G MIMO applications.

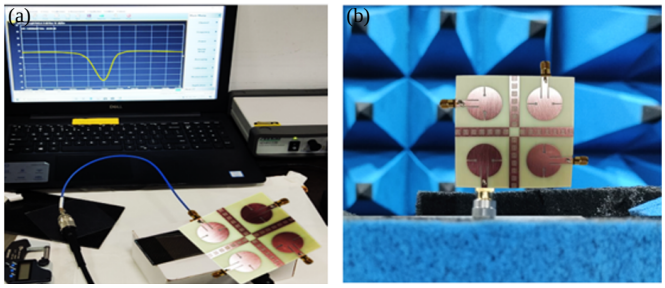

FIGURE 32. The hardware measurement setup of MIMO antenna. (a) VNA setup, (b) anechoic chamber.

3. CONCLUSION

In this paper, we have successfully designed and developed a miniaturized Multiple-Input Multiple-Output (MIMO) antenna tailored for sub-6 GHz 5G applications. By utilizing characteristic mode analysis and strategically introducing slots in the patch, we achieved orthogonal mode separation, which effectively minimized cross polarization. Further bandwidth enhancement was attained through slot loading in the ground plane. To ensure superior isolation between antenna elements, we employed spiral decoupling (SD) and aperture spiral decoupling (ASD) structures. The fabricated MIMO antenna, with compact dimensions of $0.32\lambda_o * 0.32\lambda_o * 0.01\lambda_o$ at 3.5 GHz, underwent experimental validation. The measurement results demonstrated excellent agreement with the simulated data, highlighting the antenna's compact design, low envelope correlation coefficient (ECC), 5.1 dBi gain, minimal channel capacity loss, and isolation greater than 20 dB between antenna elements. These findings affirm that the proposed MIMO antenna not only meets the stringent requirements for sub-6 GHz 5G applications but also stands as a promising candidate for advanced MIMO implementations in next-generation wireless communication systems. The enhanced performance characteristics, including reduced cross polarization and improved isolation, make it a robust solution for future wireless communication needs.

REFERENCES

[1] Milias, C., R. B. Andersen, P. I. Lazaridis, Z. D. Zaharis, B. Muhammad, J. T. B. Kristensen, A. Mihovska, and D. D. S. Hermansen, "Metamaterial-inspired antennas: A review of the state of the art and future design challenges," *IEEE Access*, Vol. 9, 89 846–89 865, 2021.

[2] Nadeem, I. and D.-Y. Choi, "Study on mutual coupling reduction technique for MIMO antennas," *IEEE Access*, Vol. 7, 563–586, 2018.

[3] Sokunbi, O. and H. Attia, "Dual-layer dual-patch EBG structure for isolation enhancement and correlation reduction in MIMO antenna arrays," *Progress In Electromagnetics Research C*, Vol. 100, 233–245, 2020.

[4] Krishnamoorthy, R., A. Desai, R. Patel, and A. Grover, "4 element compact triple band MIMO antenna for sub-6 GHz 5G wireless applications," *Wireless Networks*, Vol. 27, No. 6, 3747–3759, 2021.

[5] Roy, S. and U. Chakraborty, "Mutual coupling reduction in a multi-band MIMO antenna using meta-inspired decoupling network," *Wireless Personal Communications*, Vol. 114, No. 4, 3231–3246, 2020.

[6] Hao, C., H. Zheng, Y. Gu, and X.-B. Sun, "Mutual coupling reduction of MIMO antenna array using meta-FCRR," *Wireless Personal Communications*, Vol. 119, No. 4, 3435–3445, 2021.

[7] Fakharian, M. M., M. Alibakhshikenari, C. H. See, and R. Abd-Alhameed, "A high gain multiband offset MIMO antenna based on a planar log-periodic array for Ku/K-band applications," *Scientific Reports*, Vol. 12, No. 1, 4044, 2022.

[8] Hussein, H., F. Atasoy, and T. A. Elwi, "Miniaturized antenna array-based novel metamaterial technology for reconfigurable MIMO systems," *Sensors*, Vol. 23, No. 13, 5871, 2023.

[9] Veeramani, A., A. S. Arezomand, J. Vijayakrishnan, and F. B. Zarrabi, "Compact S-shaped EBG structures for reduction of mutual coupling," in *2015 Fifth International Conference on Advanced Computing & Communication Technologies*, 21–25, Haryana, India, Feb. 2015.

[10] Bellary, A., K. Kandasamy, and P. H. Rao, "Analysis of wave propagation models with radio network planning using dual polarized MIMO antenna for 5G base station applications," *IEEE Access*, Vol. 10, 29 183–29 193, 2022.

[11] Zhou, W., Z. Cheng, and Y. J. Guo, "A dual-polarized patch antenna with electric and magnetic coupling feed for 5G base stations," in *2020 IEEE 5th International Conference on Integrated Circuits and Microsystems (ICICM)*, 27–30, Nanjing, China, Oct. 2020.

[12] Molins-Benlliure, J., E. Antonino-Daviu, M. Cabedo-Fabrés, and M. Ferrando-Bataller, "Four-port wide-band cavity-backed antenna with isolating X-shaped block for sub-6 GHz 5G indoor base stations," *IEEE Access*, Vol. 9, 80 535–80 545, 2021.

[13] Yang, S., L. Liang, W. Wang, Z. Fang, and Y. Zheng, "Wideband gain enhancement of an AMC cavity-backed dual-polarized antenna," *IEEE Transactions on Vehicular Technology*, Vol. 70, No. 12, 12 703–12 712, 2021.

[14] Li, M., X. Chen, A. Zhang, and A. A. Kishk, "Dual-polarized broadband base station antenna backed with dielectric cavity for 5G communications," *IEEE Antennas and Wireless Propagation Letters*, Vol. 18, No. 10, 2051–2055, 2019.

[15] Komandla, M. V., G. Mishra, and S. K. Sharma, "Investigations on dual slant polarized cavity-backed massive MIMO antenna panel with beamforming," *IEEE Transactions on Antennas and Propagation*, Vol. 65, No. 12, 6794–6799, 2017.

[16] Wu, C., J. Qiu, N. Wang, O. Denisov, S. Qiu, and B. Liu, "Bandwidth enhancement of broadband dual-polarized dipole antenna for 5G base station," in *2021 IEEE 4th International Conference on Electronics Technology (ICET)*, 660–663, Chengdu, China, May 2021.

[17] Çiydem, M., "A low-profile dual-polarized antenna with high isolation and high front-to-back ratio for 5G base stations," *The Applied Computational Electromagnetics Society Journal (ACES)*, 1229–1236, 2021.

[18] Alibakhshikenari, M., B. S. Virdee, C. H. See, P. Shukla, S. M. Moghaddam, A. U. Zaman, S. Shafqaat, M. O. Akinsolu, B. Liu, J. Yang, *et al.*, "Dual-polarized highly folded bowtie antenna with slotted self-grounded structure for sub-6 GHz 5G applications," *IEEE Transactions on Antennas and Propagation*, Vol. 70, No. 4, 3028–3033, 2022.

[19] Yang, S., M. An, H. Zhai, Y. Zeng, and Z. Wang, "Decoupling of wideband dual-polarized base station antennas for sub-6 GHz applications," in *2020 International Conference on Microwave and Millimeter Wave Technology (ICMMT)*, 1–3, Shanghai, China, Sep. 2020.

[20] Al-Tarifi, M. A., M. S. Sharawi, and A. Shamim, "Massive MIMO antenna system for 5G base stations with directive ports and switched beamsteering capabilities," *IET Microwaves, Antennas & Propagation*, Vol. 12, No. 10, 1709–1718, 2018.

[21] Balanis, C. A., *Antenna Theory: Analysis and Design*, John Wiley & Sons, New York, 2015.

[22] Lohar, F. L., I. B. Sharma, V. Katewa, and M. M. Sharma, "T-shaped tri-band antenna based on characteristic mode analysis for satellite applications," *Progress In Electromagnetics Research C*, Vol. 115, 65–80, 2021.

[23] Lohar, F. L., C. Dhote, Y. Solunke, and N. K. Suyan, "Design of circularly polarized IRNSS receiver antenna using characteristic mode analysis," in *2019 IEEE Indian Conference on Antennas and Propogation (InCAP)*, 1–5, Ahmedabad, India, Dec. 2019.

[24] Suyan, N. K., F. L. Lohar, Y. Solunke, and C. Dhote, "Design of compact size tri-band stacked patch antenna for GPS and IRNSS applications," in *Intelligent Learning for Computer Vision, CIS 2020. Lecture Notes on Data Engineering and Communications Technologies*, Vol. 61, 501–509, Springer, Singapore, 2020.

[25] Singh, J., F. L. Lohar, and B. S. Sohi, "Design of dual band millimeter wave antenna using SIW material for 5G cellular network applications," *Materials Today: Proceedings*, Vol. 45, 5405–5409, 2021.

[26] Wu, A., Y. Tao, P. Zhang, Z. Zhang, and Z. Fang, "A compact high-isolation four-element MIMO antenna with asymptote-shaped structure," *Sensors*, Vol. 23, No. 5, 2484, 2023.

[27] Tran, H.-H., T. T.-L. Nguyen, and T. N. Thi, "Two closely spaced microstrip patches with high isolation for full-duplex/MIMO applications," *PLoS One*, Vol. 18, No. 10, e0290980, 2023.

[28] Naik, A. A., T. Ali, P. R. Mane, R. M. David, S. Pathan, J. Anguera, *et al.*, "High-isolation wide-band four-element MIMO antenna covering Ka-band for 5G wireless applications," *IEEE Access*, Vol. 11, 123 030–123 046, 2023.

[29] Mahto, S. K., A. K. Singh, R. Sinha, M. Alibakhshikenari, S. Khan, and G. Pau, "High isolated four element MIMO antenna for ISM/LTE/5G (sub-6 GHz) applications," *IEEE Access*, Vol. 11, 82 946–82 959, 2023.

[30] Hu, W., Q. Li, H. Wu, Z. Chen, L. Wen, W. Jiang, and S. Gao, "Dual-band antenna pair with high isolation using multiple orthogonal modes for 5G smartphones," *IEEE Transactions on Antennas and Propagation*, Vol. 71, No. 2, 1949–1954, 2023.

[31] Deng, C., X. Cao, D. Li, and W. Yu, "Compact dual-band MIMO antenna with shared decoupling structure for 5G mobile terminals," *IEEE Antennas and Wireless Propagation Letters*, Vol. 22, No. 6, 1281–1285, 2023.

[32] Abubakar, H. S., Z. Zhao, M. E. Munir, W. U. K. Tareen, B. Wang, S. H. Kiani, and T. Ali, "Enhanced smartphone connectivity: dual-band MIMO antenna with high isolation and low ECC," *Physica Scripta*, Vol. 99, No. 6, 065524, 2024.

[33] Tran, H.-H., T. T.-L. Nguyen, H.-N. Ta, and D.-P. Pham, "A metasurface-based MIMO antenna with compact, wideband, and high isolation characteristics for sub-6 GHz 5G applications," *IEEE Access*, Vol. 11, 67 737–67 744, 2023.

[34] Nguyen-Manh, H., D.-P. Pham, G. Nguyen-Hoai, H.-H. Tran, and N. Q. Dinh, "A design of MIMO antenna with high isolation and compact size characteristics," *IEEE Access*, Vol. 11, 93 948–93 955, 2023.

[35] Wang, Z., W. Ren, W. Nie, W. Mu, and C. Li, "Design of three-band two-port MIMO antenna for 5G and future 6G applications based on fence-shaped decoupling structure," *Progress In Electromagnetics Research C*, Vol. 134, 249–261, 2023.

[36] Abbas, A., N. Hussain, M. A. Sufian, W. A. Awan, J. Jung, S. M. Lee, and N. Kim, "Highly selective multiple-notched UWB-MIMO antenna with low correlation using an innovative parasitic decoupling structure," *Engineering Science and Technology, An International Journal*, Vol. 43, 101440, 2023.

[37] Tashvigh, V. and M. Kartal, "A dual-sense CP MIMO antenna using decoupling structure with improved isolation," *AEU — International Journal of Electronics and Communications*, Vol. 175, 155065, 2024.

[38] Brizi, D., N. Fontana, F. Costa, R. Matera, G. Tiberi, A. Galante, M. Alecci, and A. Monorchio, "Design of distributed spiral resonators for the decoupling of MRI array coils," in *2020 14th European Conference on Antennas and Propagation (EuCAP)*, 1–3, Copenhagen, Denmark, Mar. 2020.

[39] Garbacz, R. and R. Turpin, "A generalized expansion for radiated and scattered fields," *IEEE Transactions on Antennas and Propagation*, Vol. 19, No. 3, 348–358, 2003.